Eur. Phys. J. B **40**, 463–470 (2004)
DOI: 10.1140/epjb/e2004-00285-7

THE EUROPEAN PHYSICAL JOURNAL B

Magnetization reversal measurements in mesoscopic amorphous magnets by magneto-optical Kerr effect

R. Morales, J.I. Martín[a], M. Vélez, and J.M. Alameda

Depto. Física, Universidad de Oviedo, c/ Calvo Sotelo s/n, 33007 Oviedo, Spain

Received 11 December 2003 / Received in final form 16 June 2004
Published online 24 September 2004 –

Abstract. A magneto-optical setup based on the transverse Kerr effect has been designed to study the magnetization reversal processes by vector magnetometry in arrays of magnetic nanostructures with a reduced total volume. This system allows the measurement of both the parallel and perpendicular to the field components of the magnetization. It has been used to analyze the behavior of amorphous Co_xSi_{1-x} lines fabricated by electron beam lithography that present a very well defined shape induced uniaxial anisotropy. When the field is applied near to the hard direction, coherent rotation processes are found to occur with a collapse of this reversal mode at fields very close to the hard axis that allows to estimate the very low anisotropy dispersion of these samples. The analysis of the vector hysteresis loops reveals that the magnetization switches via an incoherent process that starts prior to the Stoner-Wohlfarth instability and that can be described in terms of a localized curling-like reversal mode.

PACS. 75.75.+a Magnetic properties of nanostructures – 75.60.Jk Magnetization reversal mechanisms – 75.50.Kj Amorphous and quasicrystalline magnetic materials

1 Introduction

The fast development of different lithography methods has allowed the fabrication of high quality ordered magnetic nanostructures in the last few years. The combination of some techniques, as electron beam lithography, X-ray lithography or laser interference lithography, with several lithography procedures, as lift-off, etching or electroplating, has led to the preparation of patterned nanoelements made of a wide variety of magnetic materials and with different structural properties, such as polycrystalline, single-crystalline or amorphous [1–5]. These small nanostructures are very interesting for application purposes in magnetic recording and are also intensively studied from the basic point of view because they can reveal novel properties related with their mesoscopic dimensions.

On the other hand, the study of the magnetic properties of these small nanostructures can become difficult due to the reduced volume of the nanoelements and, therefore, to their small magnetic moment. Thus, the conventional magnetization measurement techniques are often not suitable to characterize them, unless the nanostructures are patterned in arrays over very large areas. To address this issue, different measurement methods have been designed and developed. Some of these techniques that allow the analysis of arrays of particles with small dimensions are magnetic force microscopy (MFM) [6], electron holography [7], Lorentz microscopy [8], Hall magnetometry [9], magneto-optical Kerr effect [10,11] and micron superconducting quantum interference device (μ-SQUID) [12]. However, important characteristics of the magnetization reversal processes remain unsolved as these measurements do not usually give a complete description of the magnetization in the magnetic nanostructures when a hysteresis loop is measured. One interesting approach to analyze the domain structure of periodic nanostructures is the analysis and modeling of the magnetooptical response of the light diffracted by the samples [13]. On the other hand, in order to make a clear determination of the presence of rotation processes in the magnetization reversal in bulk materials and unpatterned thin films, it is often very helpful to measure not only the usual hysteresis loop of the component of the magnetization that is parallel to the applied magnetic field (i.e., the longitudinal component $M_{\parallel}$), but also the hysteresis loop of the component of the magnetization that is perpendicular to the applied field (i.e., the transverse component $M_{\perp}$) [14–17]. Vector magnetometry has also been used to study the magnetic behavior of continuous magnetic films with arrays of submicrometric holes patterned over extended areas [18] but, up to our knowledge, this kind of technique has not been implemented yet to analyze magnetic nanostructures such as lines or dots with a reduced total volume.

[a] e-mail: jmartin@condmat.uniovi.es

In this work, we present a specifically designed vector magnetometry setup that allows the measurement of the hysteresis loop of any component of the magnetization, in particular of both the longitudinal and transverse magnetization components, within magnetic nanostructures with the magneto-optical transverse Kerr effect (MOKE). Then, it has been used to analyze the magnetization reversal in amorphous Co_xSi_{1-x} lines of submicron width. It is worthwhile to note that the fabrication and study of nanostructures of amorphous magnetic materials are relevant as these materials usually present low coercive and anisotropy fields, and a magnetic anisotropy that can be easily tailored and controlled in the fabrication process.

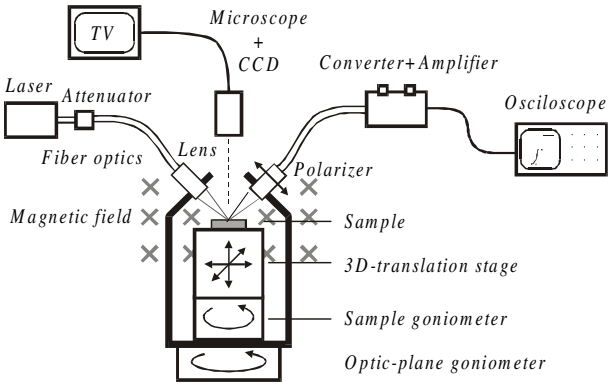

Fig. 1. Sketch of the experimental set-up used for the Kerr effect measurements of the hysteresis loops of the different magnetization components of the microstructure.

2 Experimental

The designed experimental setup for the transverse MOKE measurements is schematically shown in Figure 1. The incident light is produced by a stabilized diode laser and it is focused onto the sample holder through an optical fiber that ends in a lens. The lens has been chosen to produce a focus diameter of about 300 μm on the sample, so that the magnetic signal of a small patterned area can be characterized. An attenuator allows the regulation of the laser intensity. The light reflected by the magnetic sample is collected in an optical system with a polarizer and a lens, so that it is focused into another optical fiber. The signal is then converted with a photodiode, amplified, and sent to a digital oscilloscope where it is analyzed.

The transverse MOKE used in this set-up is characterized by a small change in the reflectance of the light linearly polarized in the optical plane due to the magnetization component perpendicular to it [19]. For this reason, a properly oriented polarizer must be introduced in light path. It could have been placed either in the path of the incoming light or, as was finally done due to geometrical convenience, after the light is reflected from the sample. This second option implies that there could be a small contribution to the signal due to the longitudinal Kerr effect (that induces a rotation in the polarization plane of the incident light together with an ellipticity due to the magnetization component parallel to the optical plane). However, any intensity changes due to this effect would be even in the magnetization, different from the odd transverse MOKE, and would simply add up to other even contributions always present in the measurements due to higher order magnetooptical effects [19,20]. In any case, test measurements have been performed to confirm that, to the system accuracy, there was not a significant difference between the loops taken with the polarizer situated either before or after the light is reflected from the sample.

The sample holder, made with a non-magnetic material, allows the lateral and vertical movement through a 3D precision translator, and the in-plane sample rotation with a goniometer. Also, the whole sample holder together with the optical lenses system is mounted on a different goniometer; therefore, the optical plane can be rotated in the presence of the magnetic field once the light is focused onto the desired array of magnetic nanostructures. This technical possibility allows the measurement of the projection of the magnetization along any desired direction, which is used in this case to obtain both components ($M_{\parallel}$ and $M_{\perp}$) of the magnetization. The total size of the whole optical system of this setup is smaller than 5 cm, so that it can be placed in the gap between the pole pieces of a electromagnet that produces a magnetic field, parallel to the sample plane, of up to 3 kOe. The particular magnetic nanostructured array to be measured can be located at the spot of the laser, by using the 3D translator, with the help of a external optical microscope connected to a digital camera.

The array of amorphous Co_xSi_{1-x} lines has been fabricated by using electron beam lithography in combination with a lift-off process, as reported elsewhere [21]. The Co_xSi_{1-x} alloy is obtained by co-sputtering from pure Co and Si targets with a composition $x = 0.72$, since the structure of $Co_{72}Si_{28}$ alloy films is amorphous as revealed by X-ray diffraction [22]. The dimensions of the lines are $w = 280$ nm in width, $t = 40$ nm in thickness, and $l = 250$ μm in length; the array is fabricated over a total area of 250 μm $\times$ 250 μm. The center-to-center distance of the lines is 0.75 μm, several times larger than the line width, so that the influence of the magnetostatic interaction between neighbor lines in the magnetic behavior can be neglected [5]. The fact that the magnetization of the whole array is recorded at the same time implies that the hysteresis loops obtained will be the average for the 300 lines involved. Even more, each loop presented in this work is actually the time-average over about 100 individual loops in order to improve the signal to noise ratio. It means that any sharp features that could be present in individual loops will be smeared out but it has the advantage that the statistical behavior of the array is obtained, allowing us to compare the $M_{\parallel}$ and $M_{\perp}$ loops, even if they are taken sequentially and not simultaneously.

3 Results and discussion

3.1 Magnetic characterization

The MOKE hysteresis loops of the array of amorphous lines, both $M_{\|}$ and $M_{\perp}$ components, are presented in Figure 2, for different values of the angle (θ) between the applied magnetic field and the lines direction. At $\theta = 0°$, that is, with the field applied along the lines, the $M_{\|}$ loop presents the typical characteristics of a magnetic easy axis; the magnetization state does not change significantly from the saturation (M_S) to the remanence (M_r), that is, $M_r/M_S \approx 1$, and there is a sharp jump at the coercive field that reverses the magnetization state (Fig. 2a). For magnetic fields applied close to the direction perpendicular to the lines, the characteristic behavior of a uniaxial hard axis is found in $M_{\|}$ loops (Fig. 2c for $\theta = 88°$, and Fig. 2e for $\theta = 90°$), that is, $H_C \sim 0$ and $M_r/M_S \sim 0$. It reveals that, actually, the uniaxial anisotropy induced by the shape of the lines is the dominant one. Also, from the $M_{\|}$ loop at the hard axis, $\theta = 90°$, an anisotropy field $H_K \approx 550$ Oe can be estimated which is much larger than the corresponding value in a continuous film of the same composition $H_K = 30$ Oe. Taking into account that $M_S \approx 320$ emu/cm^3 in our samples (obtained from SQUID measurements in the unpatterned $Co_{0.72}Si_{0.28}$ film), this H_K corresponds to an anisotropy energy $K = H_K M_S/2 \approx 8.8 \times 10^4$ erg/cm^3. This is in reasonable agreement with the value calculated for the shape anisotropy of the lines as $K_{sh} = {}^1/_2(N_a - N_b)M_S^2 \approx 8.0 \times 10^4$ erg/cm^3, being N_a and N_b the demagnetizing factors along the width and the length of the lines respectively. In our case, they are $N_a = 4\pi t/(w + t) = 0.5\pi$ and $N_b = 0$, considering the expressions for the demagnetizing factors of a general ellipsoid [23]. It is worth to note that these well defined uniaxial hard axis loops observed in this array of amorphous lines are not usually found in submicrometric lines [4,24–26] of polycrystalline and single crystalline materials due to the interplay of magnetocrystalline anisotropy and defect microstructure with the patterning induced shape anisotropy; in particular, polycrystalline Co_xSi_{1-x} lines of similar dimensions are found to present a clear hysteretic behavior even at the hard axis [21].

The $M_{\perp}$ loop of the amorphous Co-Si lines measured at $\theta = 0°$ presents values of the $M_{\perp}$ component very close to zero in the whole field range (Fig. 2b). On the other hand, when the field is applied close to the hard axis at $\theta = 88°$ (Fig. 2d), the $M_{\perp}$ loop shows a continuous increase in the magnetization as the field is decreased from the saturation, up to $M_{\perp}/M_S \approx 1$ for $H = 0$. It reveals that the magnetization of all the lines rotates from the saturation to the perpendicular direction to the applied field, i.e. parallel to the lines direction, at the remanence. However, the $M_{\perp}$ loop looks very different when the field is applied 2° further at $\theta = 90°$ (Fig. 2f), that is, for the precise direction perpendicular to the submicrometric lines. In this case $M_{\perp}$ is always close to 0, and only reaches values up to $M_{\perp}/M_S \approx 0.2$ in the reversal process.

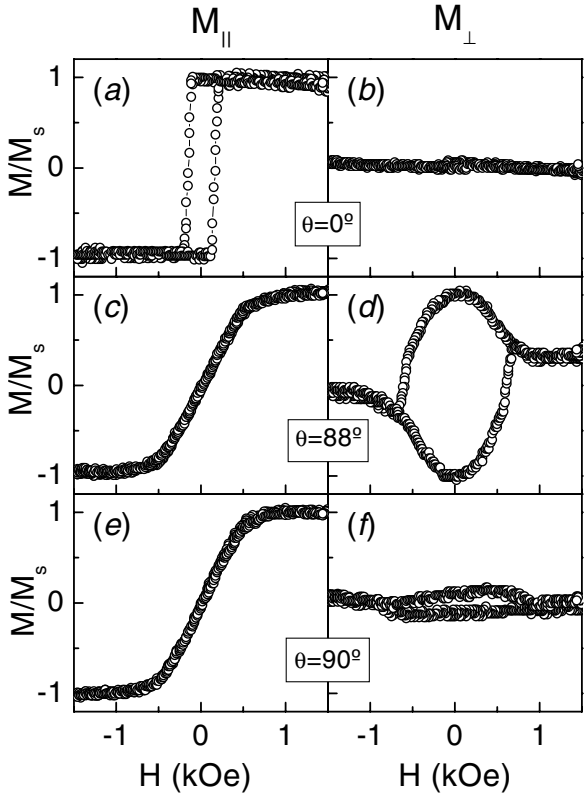

Fig. 2. MOKE hysteresis loops of the array of amorphous $Co_{72}Si_{28}$ lines for different angles between the lines and the applied magnetic field: (a), (c) and (e) correspond to the longitudinal component $M_{\|}$ and (b), (d) and (f) to the transverse component $M_{\perp}$. The loops are normalized by the saturation value.

This sensitivity of the $M_{\perp}$ loop to the details of the reversal process can be taken to full advantage by the use of normalized $M_{\perp}$ vs. $M_{\|}$ polar plots, i.e. of the angular position of the magnetization vector along the hysteresis loop, deduced from the composition of the $M_{\perp}(H)$ and $M_{\|}(H)$ curves. In the following, this vector magnetometry technique will be applied first to study the rotation processes of the magnetization for fields applied close to the hard axis and, then, the magnetization reversal mechanisms that control the lines coercive fields will be analyzed in the whole angular range.

3.2 Hard axis loops

Figure 3 shows the comparison of the $M_{\perp}$ vs. $M_{||}$ polar plots for a field applied close to the hard axis (at $\theta = 88°$) and that taken with H precisely perpendicular to the lines direction. In the first case, the polar plot presents a shape very close to a circle of radius $M/M_S = 1$, as shown in Figure 3a, indicating that, at this angle, the magnetization of the lines mostly reverses by coherent rotation from negative to positive saturation, so that the total magnitude of M does not significantly change in the process. For $\theta = 90°$ (Fig. 3b), a collapse is observed in the polar plot, similarly to the behavior found in other works

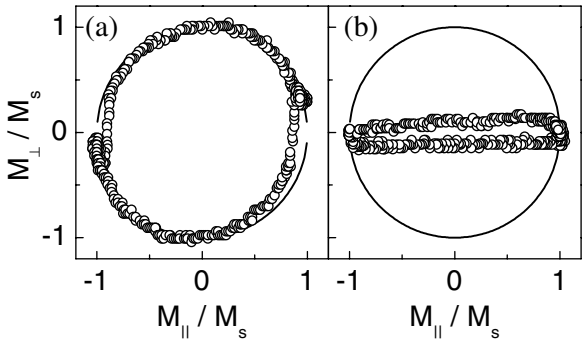

Fig. 3. Normalized polar plots of $M_\perp$ vs. $M_\parallel$ for different angles of the applied field to the lines: (a) $\theta = 88°$; (b) $\theta = 90°$.

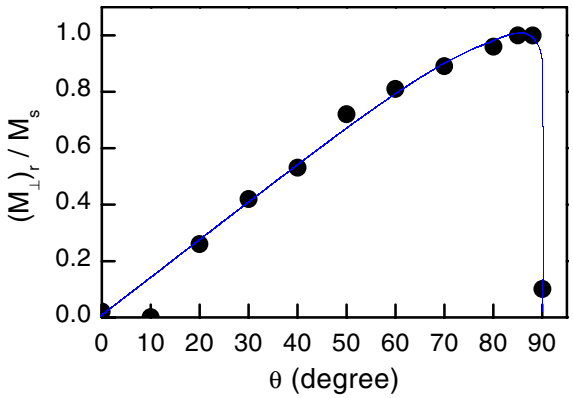

Fig. 4. Angular dependence of the normalized value of the transverse magnetization at the remanence $(M_\perp)_r/M_S$.

in continuous magnetic films when the field is applied in the direction of the hard axis [14]. It is related with the frustration in the sense of the magnetization rotation because the anisotropy torque is zero at this angular position. Then, any dispersion in the distribution of local easy axes of the sample, that can arise due to microstructural inhomogeneities, makes the sample split into domains resulting in a total reduction of $M_\perp$.

Then, the width of the anisotropy axes distribution can be estimated from the angular dependence of the normalized $M_\perp$ at the remanence, $(M_\perp)_r/M_S$, shown in Figure 4. First, as the field is deviated from the easy axis up to $\theta = 88°$, a continuous increase in $(M_\perp)_r/M_S$ is observed up to a maximum value $(M_\perp)_r/M_S$ ($88° \approx 1$. This is characteristic of a coherent rotation of the magnetization towards the lines directions so that $(M_\perp)_r/M_S = \sin\theta$. Only then, in a very narrow angular range, the $(M_\perp)_r/M_S$ curve does decrease steeply as the angle is further increased up to $\theta = 90°$. This indicates that in this array of amorphous Co_xSi_{1-x} wires the anisotropy dispersion is less than the smallest angular interval used in the measurements $\Delta\theta = 2°$. This small angular dispersion is in good agreement with the fact that the amorphous microstructure of the lines results in a very high degree of homogeneity at the submicrometric scale, since disorder occurs at the much finer length scale of interatomic distances.

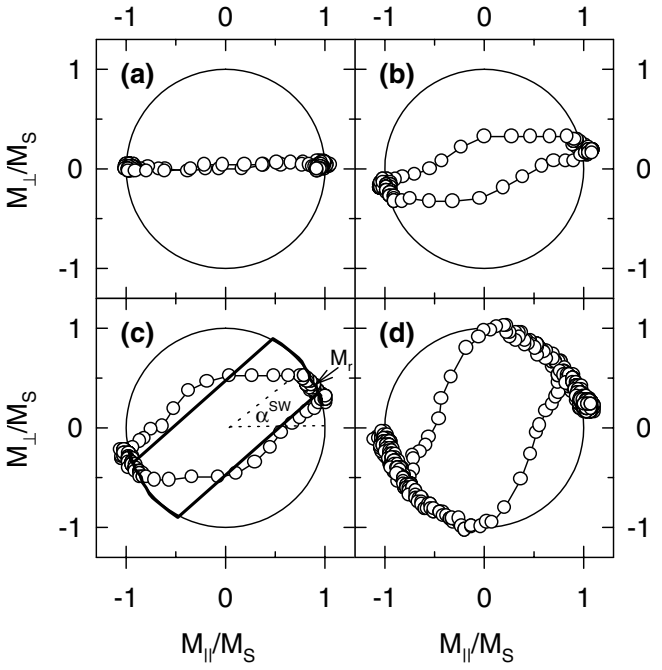

Fig. 5. Normalized polar plots of the vector hysteresis loops $M_\perp$ vs. $M_\parallel$ for different angles of the applied field to the lines: (a) $\theta = 0°$; (b) $\theta = 20°$; (c) $\theta = 30°$, (d) $\theta = 60°$. Solid line in panel (c) is the calculated Stoner-Wolfarth hysteresis loop. Also indicated are the positions corresponding to the remanence and to the nucleation of the switching process.

3.3 Magnetization switching processes

Coherent rotation processes are also present in the hysteresis loops measured for angles closer to the lines direction as shown in Figure 5, where the normalized $M_\perp$ vs. $M_\parallel$ plots can be seen for $\theta = 0°$, $20°$, $30°$ and $60°$. In all the cases, except for fields exactly along the easy axis, there is a portion of the loop in which, as the field is decreased from the saturation, the magnetization vector rotates along the circle of radius unity reaching the lines direction at remanence. As the field sense is inverted, this rotation process continues slightly beyond the lines until a switching process is initiated marked by the departure of the magnetization vector from the circle of radius unity. A comparison with the behavior calculated with the Stoner-Wolfarth model [14] (see solid line in Fig. 5c for $\theta = 30°$), clearly shows that the magnetization reversal process starts prior to the instability point of the coherent rotation process. Actually, in all the loops of Figure 5, the magnetization switches via an incoherent process in which the modulus of the magnetization vector is not conserved.

The two most relevant incoherent magnetization reversal processes for elongated ellipsoids are domain wall propagation and curling, each one being favored depending on the magnetic element dimensions relative to the material exchange correlation length R_0, that can be defined as $R_0 = (A/2M_S^2)^{1/2}$ being A the exchange constant.

In this case, the vector hysteresis loops does not seem compatible with the simplest mechanism involving the motion of a 180° domain wall either parallel or transverse

to the lines. This would imply the presence of two domains with magnetizations oppositely directed along the wire axis, so that the angular position of the average magnetization vector would not be altered in the reversal. Only the modulus of the magnetization would change as result of a domain wall traversing the magnetic wire and making one of the domains grow at the expense of the other. Therefore, this kind of domain wall motion process would appear as a radial line going through the center of the polar plot, which is not the case here.

There are, however, many other more complex reversal processes involving domain wall motion that do not follow this simple path in the polar plot of the magnetization and that are strongly dependent on many different sample parameters. One of the most important factors to be taken into account is magnetic anisotropy, which for the wires studied here is uniaxial, due to the shape of the lines, and with a very low degree of anisotropy dispersion (i.e. a very sharp distribution of anisotropy axes) as shown in the previous section. In the similar case of uniaxial thin films with very low anisotropy dispersion, the reversal has been proposed to occur in a three stage process [14]: first, as an increasingly negative field is applied to the sample, the magnetization, that was oriented along the easy axis at remanence, rotates up to the point of instability predicted by the Stoner-Wolfarth model ($\mathbf{M}_1$); second, domains are nucleated in which the magnetization has switched to the other extreme of the Stoner-Wohlfarth discontinuity ($\mathbf{M}_2$), which is an angular position in between the easy axis and the negative field direction, and a set of walls bisecting the two magnetization directions is created; finally, in a third step, these reversed domains grow at the expense of the others until the magnetization is oriented along $\mathbf{M}_2$ in the whole film and the coherent rotation process can proceed until the negative saturation. The global sample magnetization during the domain wall propagation step would be given by

$$\mathbf{M} = \mathbf{M}_1 + f(\mathbf{M}_2 - \mathbf{M}_1) \tag{1}$$

with f the fraction of the sample that is already reversed (i.e. $0 < f < 1$), so that the magnetization would follow a straight line in the polar plot joining the points $\mathbf{M}_1/M_\mathrm{S}$ and $\mathbf{M}_2/M_\mathrm{S}$ that mark the beginning and the end of the incoherent reversal process in the circle of radius unity (i.e. this mechanism would result essentially in an identical loop in the polar plot as that calculated by the Stoner-Wohlfarth model and shown in Fig. 5c). In real samples, the nucleation of a domain with a reversed magnetization component along the easy axis direction may occur prior to the Stoner-Wohlfarth instability. However, equation (1) would still be valid but with different angular positions of $\mathbf{M}_1/M_\mathrm{S}$ and $\mathbf{M}_2/M_\mathrm{S}$ in the polar plot. Thus, a reversal process consisting of coherent rotation of the sample until a reversed domain nucleation occurs followed by domain wall propagation would result in an incoherent process characterized by a straight line in the polar plot joining two points in the circle of radius unity. This holds as long as there are only two kinds of domains present during the reversal step which seems a plausible condition in our case, considering the well defined uniaxial anisotropy and restricted geometry of the amorphous Co-Si wires. This is, however, quite different from the behavior observed in Figures 5b and 5c, in which two different slopes appear during the incoherent process, even if we take into account that some rounding of these straight lines might be expected due to the averaging effect over the whole array of wires.

On the other hand, curling-like models have been found to be a good alternative to describe the magnetization reversal process in arrays of small magnetic wires [27]. A common procedure in order to test the validity of these curling-like models to describe magnetization reversal is to analyze the angular dependence of the coercive or switching fields [27], comparing it to the expression calculated for the switching field of an infinite cylinder of radius R [28]

$$\begin{aligned} h^\mathrm{SW} &= H^\mathrm{SW}/2\pi M_\mathrm{S} \\ &= a(1+a)/\left(a^2\sin^2\theta + (1+a)^2\cos^2\theta\right)^{1/2} \end{aligned} \tag{2}$$

where $a = -1.2049R_0^2/R^2$. This equation can be generalized to treat both ellipsoidal [28] and non ellipsoidal particles [29] as long as the appropriate normalization and demagnetizing factors are taken into account.

If standard $M_\parallel$ hysteresis loops are used, this kind of analysis is only valid in a limited angular range around the easy axis in which the coercive field can be identified with the switching field. For higher angles between the field and the easy axis the coherent rotation process extends beyond the direction perpendicular to the applied field (where $M_\parallel = 0$ and, therefore, $H = H_\mathrm{C}$) and the switching process is initiated only after $M_\parallel$ has already reversed its sign, so that $H^\mathrm{SW} > H_\mathrm{C}$ (see, e.g. the vector hysteresis loop obtained for $\theta = 70°$ shown in the inset of Fig. 6a). This departure of the switching process from coercivity can be analyzed in more detail by considering the angular dependence of the components of the magnetization vector at the start of the incoherent switching process $M_\parallel^\mathrm{SW}/M_\mathrm{S}$ and $M_\perp^\mathrm{SW}/M_\mathrm{S}$. As the angle increases from $\theta = 0°$, $M_\parallel^\mathrm{SW}/M_\mathrm{S}$ decreases from unity and changes sign for θ close to 60°, indicating that beyond this point H_C cannot be identified with the switching field anymore.

On the other hand, the information contained in the vector hysteresis loops can be used to test the predictions of the curling model in the whole angular range $0° < \theta < 180°$. A good parameter to characterize the reversal mechanism is found to be the angle α^SW between the magnetization and the applied field at the nucleation of the incoherent switching process, i.e. $\alpha^\mathrm{SW} = \tan^{-1}(M_\perp^\mathrm{SW}/M_\parallel^\mathrm{SW})$, shown in Figure 6b as a function of the angle between the applied field and the lines direction.

For an infinite cylinder, the condition for the nucleation of a curling process is given by the equation [28]

$$h^\mathrm{SW}\cos\alpha^\mathrm{SW} = \sin^2\left(\theta - \alpha^\mathrm{SW}\right) + a \tag{3}$$

where $(\theta - \alpha^\mathrm{SW})$ is the angle between the magnetization and the lines direction and the term a accounts for the exchange stiffness of the curling mode. This has to be

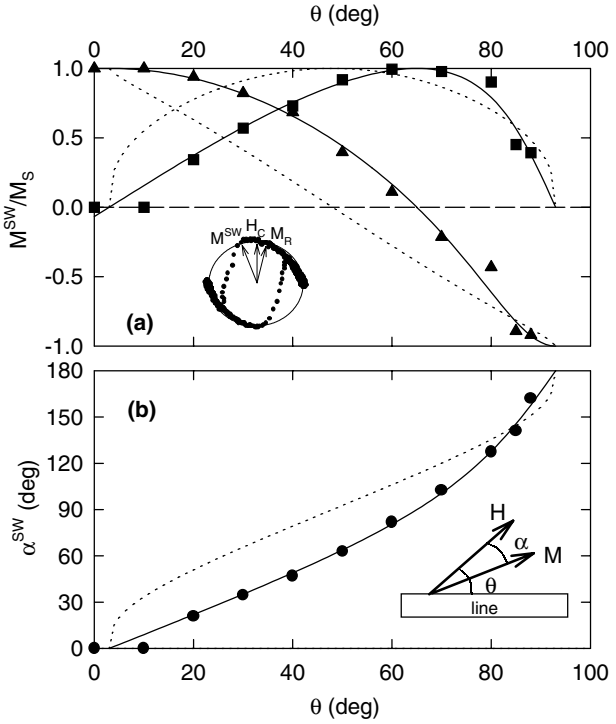

Fig. 6. (a) Dependence of the normalized magnetization components at the nucleation of the switching process $M_{\parallel}^{\mathrm{SW}}/M_{\mathrm{S}}$ (triangles) and $M_{\perp}^{\mathrm{SW}}/M_{\mathrm{S}}$ (squares) as a function of the angle θ between the field and the lines direction. Inset shows a polar plot measured for $\theta = 70^{\circ}$ with a sketch of the angular positions of the magnetization at the most relevant points in the hysteresis loop: remanence (M_{R}), coercivity ($M \perp H$ and $H = H_{\mathrm{C}}$) and switching (M^{SW}). (b) Dependence of the angle α^{SW} between the magnetization vector and the applied field at the nucleation of the switching process as a function of θ. Dashed lines correspond to the calculated behavior for the Stoner-Wolfarth model and solid lines are a fit to the predictions of the curling model with $a = -0.21$ and an angular offset $\theta_0 = 3^{\circ}$. Inset shows a sketch of the different angles involved.

compatible with the equilibrium condition of the minimum magnetostatic energy

$$h^{\mathrm{SW}} \sin \alpha^{\mathrm{SW}} = {}^1\!/_2 \sin\left[2\left(\theta - \alpha^{\mathrm{SW}}\right)\right]. \tag{4}$$

These two equations can be solved for $\sin \alpha^{\mathrm{SW}}$ and $\cos \alpha^{\mathrm{SW}}$ with the following result

$$\begin{aligned} \sin \alpha^{\mathrm{SW}} &= M_{\perp}^{\mathrm{SW}}/M_{\mathrm{S}} \\ &= \sin\theta \cos\theta / \left[a^2 \sin^2\theta + (1+a)^2 \cos^2\theta\right]^{1/2} \end{aligned} \tag{5a}$$

$$\begin{aligned} \cos \alpha^{\mathrm{SW}} &= M_{\parallel}^{\mathrm{SW}}/M_{\mathrm{S}} \\ &= \left(a + \cos^2\theta\right) / \left[a^2 \sin^2\theta + (1+a)^2 \cos^2\theta\right]^{1/2} \end{aligned} \tag{5b}$$

so that

$$\alpha^{\mathrm{SW}} = \tan^{-1}\left[\sin\theta \cos\theta / (a + \cos^2\theta)\right]. \tag{6}$$

The solid lines in Figures 6a and 6b correspond to a fit of the experimental data to equations (5) and (6) with $a = -0.21$. An offset angle $\theta_0 = 3^{\circ}$ had to be introduced that is well within the experimental precision. The very good agreement found implies that curling-like processes are responsible for the nucleation of the incoherent switching process in these $\mathrm{Co}_x\mathrm{Si}_{1-x}$ lines in almost the whole angular range. The angular dependence of $M_{\perp}^{\mathrm{SW}}/M_{\mathrm{S}}$, $M_{\parallel}^{\mathrm{SW}}/M_{\mathrm{S}}$, and α^{SW} for the Stoner-Wohlfarth model has also been calculated for comparison (dashed lines in Fig. 6) using equation (4) together with the instability condition for the coherent rotation of the magnetization [14]

$$h^{\mathrm{SW}} \cos \alpha^{\mathrm{SW}} = -\cos\left[2\left(\theta - \alpha^{\mathrm{SW}}\right)\right]. \tag{7}$$

In this case, the calculated $\alpha^{\mathrm{SW}}(\theta)$ curve lies above the experimental data and the calculated curve for curling-like reversal except for angles very close to the hard axis ($\theta \leq 88^{\circ}$), clearly showing the reason why curling processes are preferred as switching mode in these structures.

From the obtained value of a, the material exchange correlation length can be estimated as $R_0 = R^*(-a/1.2049)^{1/2} = 25$ nm. The effective radius $R^* = (tw/\pi)^{1/2} = 60$ nm is derived from the condition that the results from non ellipsoidal particles (such as the lines with a rectangular section studied here) should be renormalized to the corresponding ellipsoid of the same volume [29]. This gives a value of the exchange constant $A = 2R_0^2 M_{\mathrm{S}}^2 = 1.3 \times 10^{-6}$ erg/cm that is of the same order of magnitude as reported values for other Co based amorphous alloys [30].

Now, it is interesting to compare the calculated $h^{\mathrm{SW}}(\theta)$ for a curling process using the parameter a obtained from the previous fits and equation (2) with the experimental switching field H^{SW}, i.e. that corresponding to the start of the switching process in the magnetization polar plot (see inset of Fig. 6a). The agreement found for the angular dependence is quite good up to 80° as shown in Figure 7 where both fields have been plotted normalized by their easy axis value. However, their absolute values are quite different: an estimate of the easy axis switching field predicted by curling using equation (2) would give $H_{\mathrm{curling}}^{\mathrm{SW}}(0) = 422$ Oe, much larger than the experimental $H_{\mathrm{experimental}}^{\mathrm{SW}}(0) = 95$ Oe. These differences have already been observed in Ni nanowires [27], and can be attributed [31] to the localization of the curling mode in a volume much smaller than the whole magnetic line due to the presence of small inhomogeneities such as anisotropy fluctuations related to the material microstructure. In that sense, the values of the exchange constant A and correlation length R_0 obtained above should be considered as order of magnitude estimates only, since the actual size and shape of this localized curling volume could be significantly different from the global wire dimensions used in this calculation. Finally, once the localized curling process has been nucleated, the complete reversal of the lines would take place by the propagation of this initial nucleus in a so-called "vortex wall" [32].

Thus, the global picture of the magnetization reversal process is that of a coherent rotation of the

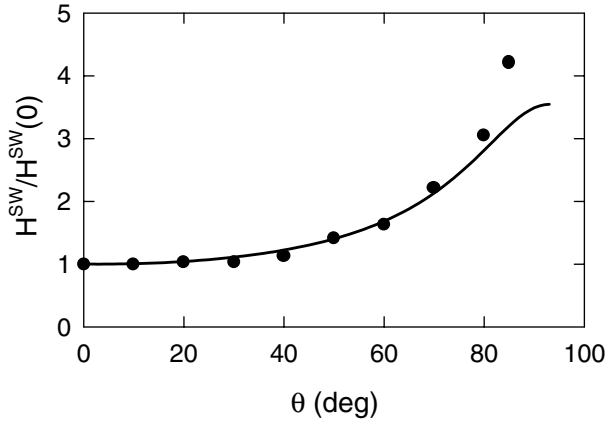

Fig. 7. Angular dependence of the switching field normalized by its easy axis value, $H^{\mathrm{SW}}(\theta)/\ H^{\mathrm{SW}}(0)$. Solid line is the calculated dependence for the curling model using equation (2) with the parameters obtained above ($a = -0.21$ and $\theta_0 = 3^\circ$).

magnetization of the wires until the nucleation of a reversed nucleus occurs through a localized curling process which, then, propagates reversing the rest of the line.

4 Conclusions

In summary, a magneto-optical setup has been designed that allows the measurement of both longitudinal and perpendicular components of the magnetization in magnetic nanostructures by transverse Kerr effect. It has been used to study the magnetization reversal processes in nanowires of amorphous Co_xSi_{1-x}, that present an uniaxial magnetic anisotropy related to the shape of the wires.

The $M_{\|}$ and $M_{\perp}$ measurements for fields applied close to the hard axis reveal that the magnetization reversal is mainly driven by coherent rotation of all the lines, with a collapse in the $M_{\perp}$ loops for field directions very close to the hard axis that allows to estimate an anisotropy dispersion of less than 2°. The vector hysteresis loops measured for different angles between the field and the lines direction show the presence of an incoherent switching process that takes place before the Stoner-Wolfarth instability is reached. The nucleation of this switching process can be described in terms of localized curling which generates a reversed nucleus that, then, propagates along the line.

These results reveal the interest in measuring the $M_{\perp}$ component in magnetic nanostructures in order to have a complete picture of the magnetization switching processes and of the sample anisotropy dispersion.

This work was supported by Spanish CICYT under grant MAT2002-04543-C02-01 and by Accion Integrada HF/2002-0170. We acknowledge useful discussions with J.L. Vicent and F. Briones.

References

1. J.F. Smyth, S. Schultz, D.R. Fredkin, D.P. Kern, S.A Rishton, H. Schmid, M. Cali, T.R. Koehler, J. Appl. Phys. **69**, 5652 (1991)
2. J.P. Spallas, A.M. Hawryluk, D.R. Kania, J. Vac. Sci. Technol. B **13**, 1973 (1995)
3. M. Hehn, K. Ounadjela, J.P. Bucher, F. Rousseaux, D. Decanini, B. Bartenlian, C. Chappert, Science **272**, 1782 (1996)
4. A.O. Adeyeye, J.A.C. Bland, C. Daboo, D.G. Hasko, Phys. Rev. B **56**, 3265 (1997)
5. M. Velez, R. Morales, J.M. Alameda, F. Briones, J.I. Martín, J.L. Vicent, J. Appl. Phys. **87**, 5654 (2000)
6. A. Gibson, S. Schultz, J. Appl. Phys. **73**, 4516 (1993)
7. R.E. Dunin-Borkowski, M.R. McCartney, B. Kardynal, D.J. Smith, J. Appl. Phys. **84**, 374 (1998)
8. S. Hefferman, J.N. Chapman, S. McVitie, J. Magn. Magn. Mater. **95**, 76 (1991)
9. A.K. Geim, S.V. Dubonos, J.G.S. Lok, I.V. Grigorieva, J.C. Maan, L.T. Hansen, P.E. Lindelog, Appl. Phys. Lett. **71**, 2379 (1997)
10. J.L. Costa-Krämer, J.I. Martín, J.L. Menendez, A. Cebollada, J.V. Anguita, F. Briones, J.L. Vicent, Appl. Phys. Lett. **76**, 3091 (2000)
11. R.P. Cowburn, D.K. Koltsov, A.O. Adeyeye, M.E. Welland, Appl. Phys. Lett. **73**, 3947 (1998)
12. W. Wendorsfer, D. Mailly, A. Benoit, J. Appl. Phys. **87**, 5094 (2000)
13. Y. Souche, V. Novosad, B. Pannetier, O. Geoffroy, J. Magn. Magn. Mater. **177-181**, 1277 (1998)
14. M. Prutton, *Thin Ferromagnetic Films* (Butterworths, London, 1964), p. 103
15. H. Rubio, S. Suarez, S. Brown, J.W. Harrell, Phys. Rev. B **64**, 094430 (2001)
16. J.W. Lee, J. Kim, S.K. Kim, J.R. Jeong, S.C. Shin, Phys. Rev. B **65**, 144437 (2002)
17. S.M. Valvidares, L.M. Alvarez-Prado, J.I. Martin, J.M. Alameda, Phys. Rev. B **64**, 134423 (2001)
18. P. Vavassori, V. Metlushko, R.M. Osgood III, M. Grimsditch, U. Welp, G. Crabtree, W. Fan, S.R.J. Brueck, B. Ilic, P.J. Hesketh, Phys. Rev. B **59**, 6337 (1999)
19. A.K. Zvezdin, V.A. Kotov, *Modern Magnetooptics and Magnetooptical Materials* (Insitute of Physics Publishing, Bristol, 1997)
20. C.N. Afonso, F. Briones, S. Girón, Solid State Commun. **43**, 105 (1982)
21. J.I. Martín, M. Vélez, R. Morales, J.M. Alameda, J.V. Anguita, F. Briones, J.L. Vicent J. Magn. Magn. Mater. **249**, 156 (2002)
22. M. Velez, S.M. Valvidares, J. Diaz, R. Morales, J.M. Alameda, IEEE Trans. Magn. **38**, 3078 (2002)
23. J.A. Osborn, Phys. Rev. **67**, 351 (1945)
24. M. Kume, A. Maeda, T. Tanuma, K. Kuroki, J. Appl. Phys. **79**, 6402 (1996)
25. A.O. Adeyeye, G. Lauhoff, J.A.C. Bland, C. Daboo, D.G. Hasko, H. Ahmed, Appl. Phys. Lett. **70**, 1046 (1997)

26. C. Shearwood, S.J. Blundell, M.J. Baird, J.A.C. Bland, M. Gester, H. Ahmed, H.P. Hughes, J. Appl. Phys. **75**, 5249 (1994)
27. J.E. Wegrowe, D. Kelly, A. Fromck, S.E. Gilbert, J.Ph. Ansermet Phys. Rev. Lett. **82**, 3681 (1999); A. Pérez-Junquera, J.I. Martín, M. Vélez, J.M. Alameda, J.L. Vicent, Nanotechnology **14**, 294 (2003); A. Nait Abdi, J.P. Bucher, Appl. Phys. Lett. **82**, 430 (2003)
28. A. Aharoni, J. Appl. Phys. **82**, 1281 (1997)
29. A. Aharoni, J. Appl. Phys. **86**, 1041 (1999)
30. A. Yelon, *Physics of Thin Films*, edited by G. Haas, R.E. Tun (Academic Press, New York, 1971), Vol. 6, p. 205
31. R. Skomski, H. Zeng, M. Zheng, D.J. Sellmyer, Phys. Rev. B **62**, 3900 (2000)
32. R. Hertel, J. Kirschner, Physica B **343**, 206 (2004); R. Wieser, U. Nowak, K.D. Usadel, Phys. Rev. B **69**, 064401 (2004); H. Forster, T. Schrefl, W. Scholz, D. Suess, V. Tsiantos, J. Fidler, J. Magn. Magn. Mater. **249**, 181 (2002)